Published for SISSA by Springer

Received: August 14, 2012
Accepted: October 16, 2012
Published: November 8, 2012

$\bar{B} \to X_s\gamma$ in the Two Higgs Doublet Model up to next-to-next-to-leading order in QCD

Thomas Hermann,[a] **Mikołaj Misiak**[b] **and Matthias Steinhauser**[a]

[a] *Institut für Theoretische Teilchenphysik, Karlsruhe Institute of Technology (KIT), D-76128 Karlsruhe, Germany*

[b] *Institute of Theoretical Physics, University of Warsaw, Hoża 69, PL-00-681 Warsaw, Poland*

E-mail: hermann@particle.uni-karlsruhe.de, mikolaj.misiak@fuw.edu.pl, matthias.steinhauser@kit.edu

Abstract: We compute three-loop matching corrections to the Wilson coefficients C_7 and C_8 in the Two Higgs Doublet Model by applying expansions for small, intermediate and large charged Higgs boson masses. The results are used to evaluate the branching ratio of $\bar{B} \to X_s\gamma$ to next-to-next-to leading order accuracy, and to determine an updated lower limit on the charged Higgs boson mass. We find $M_{H^+} \geq 380\,\text{GeV}$ at 95% confidence level when the recently completed BABAR data analysis is taken into account. Our results for the charged Higgs contribution to the branching ratio exhibit considerably weaker sensitivity to the matching scale μ_0, as compared to previous calculations.

Keywords: Higgs Physics, Rare Decays, Beyond Standard Model, B-Physics

JHEP11(2012)036

doi:10.1007/JHEP11(2012)036

Contents

JHEP11(2012)036

1 Introduction

In view of missing (to date) New Physics signals at the Large Hadron Collider (LHC), it is of utmost importance to exploit precision calculations together with precise experimental results in order to look for deviations from the Standard Model (SM). In this context, the rare decay $\bar{B} \to X_s\gamma$ constitutes one of the most important processes. It is a loop-generated Flavour-Changing-Neutral-Current (FCNC) transition, which makes it very sensitive to contributions from beyond-SM particles. Moreover, its branching ratio can be measured with an uncertainty of a few percent and, at the same time, the result can be predicted within perturbation theory with a similar uncertainty.

The current average of the measurements by CLEO [1], BELLE [2, 3] and BABAR [4–7] reads [8]

$$\mathcal{B}(\bar{B} \to X_s\gamma)|_{E_\gamma > 1.6\,\mathrm{GeV}} = (3.37 \pm 0.23) \times 10^{-4}. \tag{1.1}$$

It includes the recently updated BABAR data analysis [4–6]. The measurements have been performed with various photon energy cutoffs E_0 ranging from 1.7 to 2.0 GeV. Their average in eq. (1.1) involves an extrapolation to $E_0 = 1.6\,\mathrm{GeV}$. It can be confronted with the SM prediction based on the Next-to-Next-to-Leading Order (NNLO) QCD calculations which reads $\mathcal{B}(\bar{B} \to X_s\gamma)|_{E_\gamma > 1.6\,\mathrm{GeV}} = (3.15 \pm 0.23) \times 10^{-4}$ [9, 10].

In this paper, we consider extensions of the SM Higgs sector by a second Higgs doublet, namely the so-called Two Higgs Doublet Models (2HDMs). They are constructed in such a way that no FCNC occur at the tree level [11]. Such models have five physical scalar degrees of freedom, among which there is a charged Higgs boson $H^\pm$ that plays an important role for $\bar{B} \to X_s\gamma$. We shall consider two versions of the model, usually denoted by 2HDM type-I and type-II where, respectively, either the same or two different Higgs doublet fields couple to the up- and down-type quarks. In these models, both Higgs doublets acquire vacuum expectation values $v_{1,2}$ such that $v = \sqrt{v_1^2 + v_2^2} \simeq 246\,\mathrm{GeV}$ determines the $W^\pm$ and Z boson masses in the same way as in the SM. The ratio v_2/v_1 is denoted by $\tan\beta$.

Comparison of the experimental results for $\mathcal{B}(\bar{B} \to X_s\gamma)$ to predictions within the 2HDM type-II leads to the strongest constraint on the charged Higgs boson mass for $\tan\beta \in [1, 25]$ (see, e.g., section 5 of ref. [12]; the precise range depends on the treatment of uncertainties). So far, the constraint has been derived using only the Next-to-Leading Order (NLO) expressions for the 2HDM contributions at the electroweak scale, while the SM contributions were treated at the NNLO [10]. In the present paper, we compute the missing two- and three-loop NNLO matching coefficients in the 2HDM, and re-do the analysis to extract a lower bound on M_{H^+} from the new experimental average (1.1).

The outline of the paper is as follows: in the next section, we discuss the matching coefficients up to the three-loop order. Besides considering the 2HDM, we also re-compute the SM matching contribution, and improve the three-loop results for C_7 and C_8. In section 3, we use the new results to evaluate $\mathcal{B}(\bar{B} \to X_s\gamma)$ to the NNLO accuracy, and to extract a lower bound on M_{H^+}. Section 4 contains our conclusions.

2 Matching coefficients

2.1 Formalism

The formalism to compute the Wilson coefficients in the 2HDM can be taken over from the SM case [13, 14]. We shall follow the regularization and renormalization conventions of those papers. In particular, we adopt the effective Lagrangian and the definition of the operators P_j ($j = 1, \ldots, 8, 11$) from eqs. (2.1) and (2.2) of ref. [14]. One should note that the dipole operators P_7 and P_8 are normalized there with inverse powers of the QCD coupling constant.

Since the additional degrees of freedom of the 2HDM are all heavy, they only influence the Wilson coefficients C_i of the operators P_i. In order to incorporate the 2HDM contribution in a manner that is analogous to the SM analysis of ref. [14], we split the Wilson coefficients as

$$C_i^Q = C_i^{Q,\mathrm{SM}} + C_i^{Q,\mathrm{2HDM}}, \tag{2.1}$$

where $Q = c, t$ marks contributions from loop diagrams with virtual charm and top quarks, respectively.

Our matching calculation is performed at the renormalization scale μ_0. It is chosen to be of the same order of magnitude as masses of the particles that are being decoupled (m_t, M_W and M_{H^+}). For the NLO calculations within the SM we refer to ref. [15]. The NNLO SM contributions to $C_i^{Q,\mathrm{SM}}(\mu_0)$ have been computed in refs. [13, 14]. Suppression by m_c^2/M_W^2 makes $C_i^{c,\mathrm{2HDM}}$ negligible. In the following, we shall consider $C_i^{t,\mathrm{2HDM}}$ only. It is convenient to decompose them as follows

$$C_i^{t,\mathrm{2HDM}} = C_i^{H(0)} + \frac{\alpha_s}{4\pi} C_i^{H(1)} + \left(\frac{\alpha_s}{4\pi}\right)^2 C_i^{H(2)} + \left(\frac{\alpha_s}{4\pi}\right)^3 C_i^{H(3)} + \ldots, \tag{2.2}$$

where $C_i^{H(n)}$ is obtained from n-loop diagrams. For $i = 7, 8$, the tree-level coefficients $C_i^{H(0)}$ vanish, while $C_i^{H(1)}(\mu_0)$ and $C_i^{H(2)}(\mu_0)$ have been found in refs. [16–20]. In the present paper, we compute the three-loop corrections $C_7^{H(3)}(\mu_0)$ and $C_8^{H(3)}(\mu_0)$, which

JHEP11(2012)036

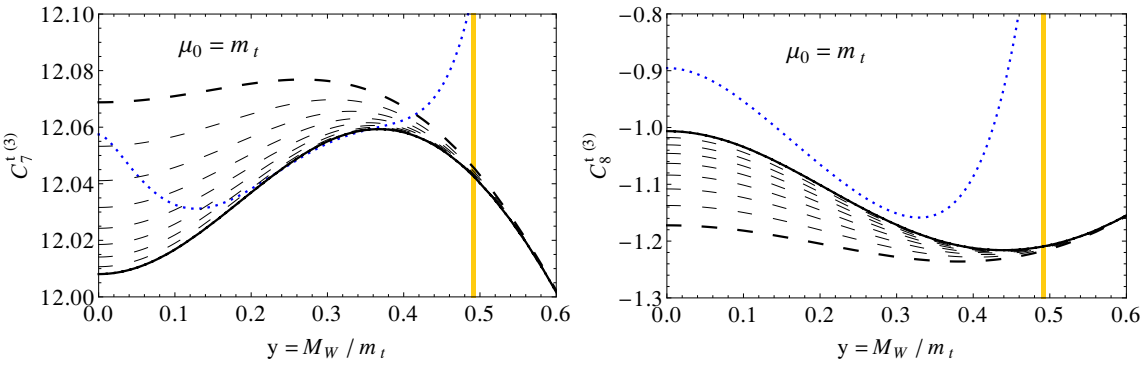

(a) (b)

Figure 1. Three-loop SM coefficients $C_7^{t(3)}(\mu_0)$ and $C_8^{t(3)}(\mu_0)$ as functions of $y = M_W/m_t$ for $\mu_0 = m_t$. Dotted lines show their expansions around $y = 0$ up to $\mathcal{O}(y^8)$. Solid lines show the expansions around $y = 1$ and include corrections up to $w^{16} = (1 - y^2)^{16}$. Dashed lines show lower orders in w. The (yellow) band represents the physically allowed region for y.

constitutes the last missing element of the 2HDM Wilson coefficient evaluation that matters for $\mathcal{B}(\bar{B} \to X_s\gamma)$ at the NNLO. Furthermore, we reproduce the two-loop corrections $C_i^{H(2)}(\mu_0)$ for $i = 3, 4, 5, 6$ that have been originally found in ref. [21] and belong to the necessary NNLO matching in the 2HDM.

In the following two subsections, we discuss our results for the Wilson coefficients in the SM and 2HDM. Several variables turn out to be of convenience in this context:

$$y = \frac{M_W}{m_t(\mu_0)}\,, \qquad w = 1 - y^2, \qquad r = \frac{m_t^2(\mu_0)}{M_{H^+}^2}\,, \qquad \bar{u} = 1 - r\,, \qquad u = 1 - \frac{1}{r}\,. \tag{2.3}$$

2.2 Standard Model

Let us begin with recalling three-loop corrections to the matching coefficients in the SM. They depend on two masses: M_W and m_t. In ref. [14], expansions of the three-loop diagrams for $M_W \ll m_t$ and $M_W \approx m_t$ have been performed. The final numerical results of that paper

$$\begin{aligned} C_7^{t(3)}(\mu_0 = m_t) &= 12.05 \pm 0.05\,, \\ C_8^{t(3)}(\mu_0 = m_t) &= -1.2 \pm 0.1\,, \end{aligned} \tag{2.4}$$

have been obtained for $y = 0.488 \pm 0.015$. They relied on convergence behaviour and agreement of the two expansions for intermediate values of M_W and m_t.

The dotted curves in figure 1 show expansions of $C_7^{t(3)}(\mu_0 = m_t)$ and $C_8^{t(3)}(\mu_0 = m_t)$ around $y = 0$ up to $\mathcal{O}(y^8)$. Results of the expansion around $y = 1$ are shown as dashed and solid lines. The thick dashed lines include terms up to w^8 that have been provided in ref. [14]. In the present calculation, we have added eight more expansion terms for $M_W \approx m_t$. They are shown in figure 1 as thin dashed lines and a solid curve that includes terms up to w^{16}.

In the case of $C_7^{t(3)}$, we observe an overlap of the two expansions for $0.2 \le y \le 0.35$, which gives us confidence that the exact curve is approximated with high accuracy by the

JHEP11(2012)036

Taylor expansion around $w = 0$ on one side, and by the asymptotic large-m_t expansion on the other. The situation for $C_8^{t(3)}$ in figure 1(b) is only slightly worse. We still observe an improvement w.r.t. ref. [14] due to the additional terms in the w expansion. The vertical bands in figure 1 correspond to the current experimentally allowed region $y = 0.492 \pm 0.003$ for $\mu_0 = m_t$. In the range $0.4 < y < 0.6$, our improved results are very well approximated (to better than 0.1%) by

$$\begin{aligned} C_7^{t(3)}(\mu_0 = m_t) &= 11.92 + 0.751\, y - 1.03\, y^2, \\ C_8^{t(3)}(\mu_0 = m_t) &= -0.764 - 2.06\, y + 2.35\, y^2, \end{aligned} \tag{2.5}$$

which is consistent with eq. (2.4) but much more accurate, and allows to substitute the updated value of y. In effect, the uncertainties get reduced by almost an order of magnitude.

As far as contributions from loops involving the charm quark are concerned, the corresponding coefficients in the range $0.4 < y < 0.6$ can be obtained with high precision from the expressions given already in ref. [14], namely

$$\begin{aligned} C_7^{c(3)}(\mu_0 = M_W) &= 1.458\, y^{-0.0338}, \\ C_8^{c(3)}(\mu_0 = M_W) &= -1.718\, y^{-0.0598}. \end{aligned} \tag{2.6}$$

They already provide a high-accuracy approximation in the physical region, so there is no need to consider higher-order terms in the expansions.

2.3 Two Higgs Doublet Model

In order to specify the notation, we provide the Lagrange density which defines interactions of the charged Higgs boson with fermions. Adopting the conventions from ref. [16], we have

$$\mathcal{L}_{H^+} = \left(2\sqrt{2} G_F\right)^{1/2} \sum_{i,j=1}^{3} \overline{u}_i (A_u m_{u_i} V_{ij} P_L - A_d\, m_{d_j} V_{ij} P_R) d_j H^+ + \text{h.c.}\,, \tag{2.7}$$

where $P_{L/R} = (1 \mp \gamma_5)/2$, V_{ij} are the Cabibbo-Kobayashi-Maskawa matrix elements, u_i and d_j are the up- and down-type quarks with masses m_{u_i} and m_{d_j}, and G_F is the Fermi constant. For the 2HDM of type-I and II, the couplings A_d and A_u take the values

$$A_u = A_d = \frac{1}{\tan\beta} \tag{2.8}$$

and

$$A_u = -\frac{1}{A_d} = \frac{1}{\tan\beta}\,, \tag{2.9}$$

respectively.

The 2HDM contributions to the Wilson coefficients in eq. (2.1) are proportional to $A_i A_j^\star$. Since the terms involving $A_d^\star$ are suppressed by the strange-quark mass, we can safely neglect them. The remaining terms can be split into two parts as follows:

$$C_i^{t,\text{2HDM}} = A_d A_u^\star\, C_{i,A_d A_u^\star}^{t,\text{2HDM}} + A_u A_u^\star\, C_{i,A_u A_u^\star}^{t,\text{2HDM}}. \tag{2.10}$$

JHEP11(2012)036

For the computation of $C_i^{t,\mathrm{2HDM}}$, we can use eq. (5.1) of ref. [14] that has been derived in the context of the SM. Its application to the 2HDM is straightforward after taking into account that, apart from the Wilson coefficients, also the electroweak counterterms (cf. eqs. (4.7) to (4.10) of [14]) and the quantities B_7 and B_8 (cf. eqs. (3.22) and (3.23) of [14]) receive additional contributions originating from the charged Higgs boson exchange. Decomposing each of these quantities as $X = X^{\mathrm{SM}} + X^{\mathrm{2HDM}}$ where X^{SM} denotes the result given in ref. [14], we obtain their 2HDM parts in $D = 4-2\epsilon$ dimensions by a simple one-loop calculation

$$\begin{aligned}
Z_{2,sb}^{t,\mathrm{2HDM}} &= \frac{m_t^2}{M_W^2} A_u A_u^\star \,\Gamma(\epsilon)\left[-\frac{1}{2} + \frac{2r-1}{2(r-1)^2}(r^\epsilon - 1) - \epsilon\,\frac{3r-1}{4(r-1)} + \mathcal{O}(\epsilon^2)\right], \\
Z_{0,sb}^{t,\mathrm{2HDM}} &= \frac{M_{H^+}^2}{M_W^2} A_d A_u^\star \, Z_{0,sb}^{t,\mathrm{SM}}|_{M_W \to M_{H^+}}, \\
B_k^{\mathrm{2HDM}} &= A_d A_u^\star \, B_k^{\mathrm{SM}}|_{M_W \to M_{H^+}}, \qquad \text{for} \quad k = 7, 8\,.
\end{aligned} \tag{2.11}$$

Both in the SM and 2HDM, the renormalization constants $Z_{0,sb}^Q$ and $Z_{2,sb}^Q$ enter the electroweak counterterm Lagrangian in the same way[1]

$$\begin{aligned}
\mathcal{L}_{\mathrm{counter}}^{\mathrm{ew}} = \frac{G_F M_W^2}{4\sqrt{2}\,\pi^2}\Bigg[& V_{cs}^* V_{cb}\left(\frac{4\pi\mu_0^2}{M_W^2}\right)^\epsilon \bar{s} P_R (i Z_{2,sb}^c \not{D} - Z_{0,sb}^c\, m_b) b \\
& + V_{ts}^* V_{tb}\left(\frac{4\pi\mu_0^2}{m_t^2}\right)^\epsilon \bar{s} P_R (i Z_{2,sb}^t \not{D} - Z_{0,sb}^t\, m_b) b\Bigg],
\end{aligned} \tag{2.12}$$

All the remaining quantities appearing in eq. (5.1) of ref. [14] are precisely the same as in the SM.

In analogy to the SM, we have to consider vacuum integrals with two mass scales (M_{H^+} and m_t) in our matching calculation. Sample diagrams up to three-loops are shown in figure 2. At the one- and two-loop levels, the calculation can be performed exactly, and one obtains C_7 and C_8 as functions of m_t/M_{H^+} [16–20]. At the three-loop level, we proceed as in ref. [14], considering expansions around $m_t \approx M_{H^+}$, for $m_t \ll M_{H^+}$, and for $m_t \gg M_{H^+}$. In the first case, a simple Taylor expansion is sufficient, and we have computed the first 16 terms in u. Calculations involving strong hierarchies require non-trivial asymptotic expansions. In these cases, five terms in r and $1/r$ have been evaluated.

For the purpose of the present analysis, we have re-evaluated the Leading Order (LO) and NLO contributions to the renormalized Wilson coefficients, confirming the results of refs. [16–20] and extending them to include higher powers in ϵ. Such an extension has been necessary for renormalization at the three-loop level. Two-loop (NNLO) Wilson coefficients of the four-quark-operators were calculated in ref. [21] for the MSSM. We have performed an independent calculation of the charged Higgs boson contribution. Full agreement has been found. We refrain from displaying here explicit analytical results for the one- and two-loop Wilson coefficients, and refer to the `Mathematica` file available from ref. [22]. Let

[1] In the corresponding eq. (4.6) of ref. [14], a factor of $\frac{M_W^2}{4\pi} e^{\gamma\epsilon}$ is missing in the global normalization, which we correct here. For clarity, the chirality projectors P_R are now displayed explicitly.

JHEP11(2012)036

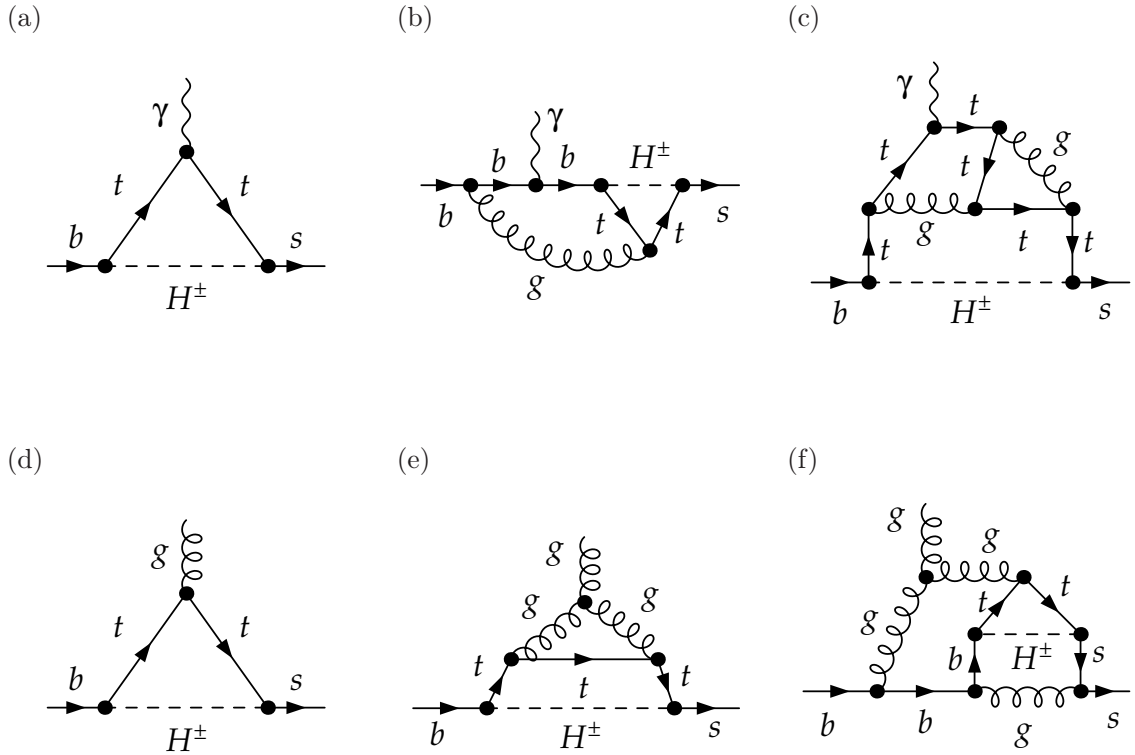

Figure 2. Sample Feynman diagrams contributing to C_7 [(a)–(c)] and C_8 [(d)–(f)] at one-, two- and three-loop order.

us only note that we set $m_t = m_t(\mu_0)$ in all those lower-order terms, which specifies our conventions for the NNLO expressions below.

At the three-loop level, we have been able to recover the dependence of C_7 and C_8 on μ_0 by applying renormalization group techniques to the analytical one- and two-loop results. We find

$$\begin{aligned}
C^{H(3)}_{7,A_u A_u^\star}(\mu_0) = {} & C^{H(3)}_{7,A_u A_u^\star}(\mu_0 = m_t) \\
& + \ln\left(\frac{\mu_0^2}{m_t^2}\right)\Bigg[-\frac{r(67930r^4 - 470095r^3 + 1358478r^2 - 700243r + 54970)}{2187(r-1)^5} \\
& \qquad + \frac{r(10422r^4 - 84390r^3 + 322801r^2 - 146588r + 1435)}{729(r-1)^6}\ln r \\
& \qquad + \frac{2r^2(260r^3 - 1515r^2 + 3757r - 1446)}{27(r-1)^5}\mathrm{Li}_2\left(1 - \frac{1}{r}\right)\Bigg] \\
& + \ln^2\left(\frac{\mu_0^2}{m_t^2}\right)\Bigg[\frac{r(-518r^4 + 3665r^3 - 17397r^2 + 3767r + 1843)}{162(r-1)^5} \\
& \qquad + \frac{r^2(-63r^3 + 532r^2 + 2089r - 1118)}{27(r-1)^6}\ln r\Bigg], \qquad (2.13)
\end{aligned}$$

JHEP11(2012)036

$$
\begin{aligned}
C^{H(3)}_{7,A_dA_u^\star}(\mu_0) &= C^{H(3)}_{7,A_dA_u^\star}(\mu_0 = m_t) \\
&\quad + \ln\left(\frac{\mu_0^2}{m_t^2}\right)\Bigg[\frac{r(3790r^3 - 22511r^2 + 53614r - 21069)}{81(r-1)^4} \\
&\qquad + \frac{2r(-1266r^3 + 7642r^2 - 21467r + 8179)}{81(r-1)^5}\ln r \\
&\qquad - \frac{8r(139r^3 - 612r^2 + 1103r - 342)}{27(r-1)^4}\mathrm{Li}_2\left(1 - \frac{1}{r}\right)\Bigg] \\
&\quad + \ln^2\left(\frac{\mu_0^2}{m_t^2}\right)\Bigg[\frac{r(284r^3 - 1435r^2 + 4304r - 1425)}{27(r-1)^4} \\
&\qquad + \frac{2r(63r^3 - 397r^2 - 970r + 440)}{27(r-1)^5}\ln r\Bigg], \qquad (2.14)
\end{aligned}
$$

$$
\begin{aligned}
C^{H(3)}_{8,A_uA_u^\star}(\mu_0) &= C^{H(3)}_{8,A_uA_u^\star}(\mu_0 = m_t) \\
&\quad + \ln\left(\frac{\mu_0^2}{m_t^2}\right)\Bigg[\frac{r(51948r^4 - 233781r^3 + 48634r^2 - 698693r + 2452)}{1944(r-1)^6}\ln r \\
&\qquad - \frac{r(522347r^4 - 2423255r^3 + 2706021r^2 - 5930609r + 148856)}{11664(r-1)^5} \\
&\qquad + \frac{r^2(481r^3 - 1950r^2 + 1523r - 2550)}{18(r-1)^5}\mathrm{Li}_2\left(1 - \frac{1}{r}\right)\Bigg] \\
&\quad + \ln^2\left(\frac{\mu_0^2}{m_t^2}\right)\Bigg[\frac{r(-259r^4 + 1117r^3 + 2925r^2 + 28411r + 2366)}{216(r-1)^5} \\
&\qquad - \frac{r^2(139r^2 + 2938r + 2683)}{36(r-1)^6}\ln r\Bigg], \qquad (2.15)
\end{aligned}
$$

$$
\begin{aligned}
C^{H(3)}_{8,A_dA_u^\star}(\mu_0) &= C^{H(3)}_{8,A_dA_u^\star}(\mu_0 = m_t) + \ln\left(\frac{\mu_0^2}{m_t^2}\right)\Bigg[\frac{r(1463r^3 - 5794r^2 + 5543r - 15036)}{27(r-1)^4} \\
&\qquad + \frac{r(-1887r^3 + 7115r^2 + 2519r + 19901)}{54(r-1)^5}\ln r \\
&\qquad + \frac{r(-629r^3 + 2178r^2 - 1729r + 2196)}{18(r-1)^4}\mathrm{Li}_2\left(1 - \frac{1}{r}\right)\Bigg] \\
&\quad + \ln^2\left(\frac{\mu_0^2}{m_t^2}\right)\Bigg[\frac{r(259r^3 - 947r^2 - 251r - 5973)}{36(r-1)^4} \\
&\qquad + \frac{r(139r^2 + 2134r + 1183)}{18(r-1)^5}\ln r\Bigg]. \qquad (2.16)
\end{aligned}
$$

Our results for $C_7^{H(3)}(\mu_0 = m_t)$ and $C_8^{H(3)}(\mu_0 = m_t)$ in terms of expansions are quite lengthy. Exact values of the expansion coefficients can be found in ref. [22]. Here, we present their approximate numerical values only. Considering consecutively the regions $r \to 0$, $r \to 1$ and $r \to \infty$, we obtain (for $\mu_0 = m_t$):

$$
\begin{aligned}
C^{H(3),r\to 0}_{7,A_uA_u^\star} &= 0.9225\, r\ln^2 r + 4.317\, r\ln r - 8.278\, r \\
&\quad -20.73\, r^2\ln^3 r - 112.4\, r^2\ln^2 r - 396.1\, r^2\ln r - 480.9\, r^2 \\
&\quad -34.50\, r^3\ln^3 r - 348.2\, r^3\ln^2 r - 1292\, r^3\ln r - 1158\, r^3 \\
&\quad -23.26\, r^4\ln^3 r - 541.4\, r^4\ln^2 r - 2540\, r^4\ln r - 1492\, r^4 \\
&\quad +42.30\, r^5\ln^3 r - 412.4\, r^5\ln^2 r - 3362\, r^5\ln r - 823.0\, r^5 + \mathcal{O}(r^6), \qquad (2.17)
\end{aligned}
$$

JHEP11(2012)036

$$C^{H(3),r\to 1^-}_{7,A_uA^\star_u} = 1.283 - 0.7158\,\bar{u} - 0.3039\,\bar{u}^2 - 0.1549\,\bar{u}^3 - 0.08625\,\bar{u}^4 - 0.05020\,\bar{u}^5$$
$$-0.02970\,\bar{u}^6 - 0.01740\,\bar{u}^7 - 0.009752\,\bar{u}^8 - 0.004877\,\bar{u}^9$$
$$-0.001721\,\bar{u}^{10} + 0.0003378\,\bar{u}^{11} + 0.001679\,\bar{u}^{12} + 0.002542\,\bar{u}^{13}$$
$$+0.003083\,\bar{u}^{14} + 0.003404\,\bar{u}^{15} + 0.003574\,\bar{u}^{16} + \mathcal{O}(\bar{u}^{17})\,, \tag{2.18}$$

$$C^{H(3),r\to 1^+}_{7,A_uA^\star_u} = 1.283 + 0.7158\,u + 0.4119\,u^2 + 0.2629\,u^3 + 0.1825\,u^4 + 0.1347\,u^5$$
$$+0.1040\,u^6 + 0.08306\,u^7 + 0.06804\,u^8 + 0.05688\,u^9 + 0.04833\,u^{10}$$
$$+0.04163\,u^{11} + 0.03625\,u^{12} + 0.03188\,u^{13} + 0.02827\,u^{14} + 0.02525\,u^{15}$$
$$+0.02269\,u^{16} + \mathcal{O}(u^{17})\,, \tag{2.19}$$

$$C^{H(3),r\to\infty}_{7,A_uA^\star_u} = 3.970 - 8.753\frac{\ln r}{r} + 15.35\frac{1}{r} - 38.12\frac{\ln r}{r^2} + 47.09\frac{1}{r^2} - 103.8\frac{\ln r}{r^3}$$
$$+79.15\frac{1}{r^3} - 168.3\frac{\ln r}{r^4} + 24.41\frac{1}{r^4} - 72.13\frac{\ln r}{r^5} - 274.2\frac{1}{r^5} + \mathcal{O}\left(\frac{1}{r^6}\right), \tag{2.20}$$

$$C^{H(3),r\to 0}_{7,A_dA^\star_u} = -20.94\,r\ln^3 r - 123.5\,r\ln^2 r - 453.5\,r\ln r - 572.2\,r$$
$$-8.889\,r^2\ln^3 r - 195.7\,r^2\ln^2 r - 870.3\,r^2\ln r - 524.1\,r^2$$
$$+19.73\,r^3\ln^3 r - 46.61\,r^3\ln^2 r - 826.2\,r^3\ln r + 166.7\,r^3$$
$$+36.08\,r^4\ln^3 r + 323.2\,r^4\ln^2 r + 169.9\,r^4\ln r + 1480\,r^4$$
$$-66.63\,r^5\ln^3 r + 469.4\,r^5\ln^2 r + 1986\,r^5\ln r + 2828\,r^5 + \mathcal{O}(r^6)\,, \tag{2.21}$$

$$C^{H(3),r\to 1^-}_{7,A_dA^\star_u} = 12.82 + 1.663\,\bar{u} + 0.7780\,\bar{u}^2 + 0.3755\,\bar{u}^3 + 0.1581\,\bar{u}^4$$
$$+0.03021\,\bar{u}^5 - 0.04868\,\bar{u}^6 - 0.09864\,\bar{u}^7 - 0.1306\,\bar{u}^8$$
$$-0.1510\,\bar{u}^9 - 0.1637\,\bar{u}^{10} - 0.1712\,\bar{u}^{11} - 0.1751\,\bar{u}^{12}$$
$$-0.1766\,\bar{u}^{13} - 0.1763\,\bar{u}^{14} - 0.1748\,\bar{u}^{15} - 0.1724\,\bar{u}^{16} + \mathcal{O}(\bar{u}^{17})\,, \tag{2.22}$$

$$C^{H(3),r\to 1^+}_{7,A_dA^\star_u} = 12.82 - 1.663\,u - 0.8852\,u^2 - 0.4827\,u^3 - 0.2976\,u^4 - 0.2021\,u^5$$
$$-0.1470\,u^6 - 0.1125\,u^7 - 0.08931\,u^8 - 0.07291\,u^9 - 0.06083\,u^{10}$$
$$-0.05164\,u^{11} - 0.04446\,u^{12} - 0.03873\,u^{13} - 0.03407\,u^{14} - 0.03023\,u^{15}$$
$$-0.02702\,u^{16} + \mathcal{O}(u^{17})\,, \tag{2.23}$$

$$C^{H(3),r\to\infty}_{7,A_dA^\star_u} = 8.088 + 9.757\frac{\ln r}{r} - 12.91\frac{1}{r} + 38.43\frac{\ln r}{r^2} - 49.32\frac{1}{r^2} + 106.2\frac{\ln r}{r^3}$$
$$-78.90\frac{1}{r^3} + 168.4\frac{\ln r}{r^4} - 24.97\frac{1}{r^4} + 101.1\frac{\ln r}{r^5} + 194.3\frac{1}{r^5} + \mathcal{O}\left(\frac{1}{r^6}\right), \tag{2.24}$$

$$C^{H(3),r\to 0}_{8,A_uA^\star_u} = 0.6908\,r\ln^2 r + 3.238\,r\ln r + 0.7437\,r$$
$$-22.98\,r^2\ln^3 r - 169.1\,r^2\ln^2 r - 602.7\,r^2\ln r - 805.5\,r^2$$
$$-66.32\,r^3\ln^3 r - 779.6\,r^3\ln^2 r - 3077\,r^3\ln r - 3357\,r^3$$
$$-143.4\,r^4\ln^3 r - 2244\,r^4\ln^2 r - 10102\,r^4\ln r - 9016\,r^4$$
$$-226.7\,r^5\ln^3 r - 5251\,r^5\ln^2 r - 26090\,r^5\ln r - 19606\,r^5 + \mathcal{O}(r^6)\,, \tag{2.25}$$

JHEP11(2012)036

$$
\begin{aligned}
C_{8,A_uA_u^\star}^{H(3),r\to 1^-} &= 1.188 - 0.4078\,\bar{u} - 0.2076\,\bar{u}^2 - 0.1265\,\bar{u}^3 - 0.08570\,\bar{u}^4 - 0.06204\,\bar{u}^5 \\
&\quad -0.04689\,\bar{u}^6 - 0.03652\,\bar{u}^7 - 0.02907\,\bar{u}^8 - 0.02354\,\bar{u}^9 \\
&\quad -0.01933\,\bar{u}^{10} - 0.01605\,\bar{u}^{11} - 0.01345\,\bar{u}^{12} - 0.01137\,\bar{u}^{13} \\
&\quad -0.009678\,\bar{u}^{14} - 0.008293\,\bar{u}^{15} - 0.007148\,\bar{u}^{16} + \mathcal{O}(\bar{u}^{17})\,, \qquad (2.26)\\
C_{8,A_uA_u^\star}^{H(3),r\to 1^+} &= 1.188 + 0.4078\,u + 0.2002\,u^2 + 0.1190\,u^3 + 0.07861\,u^4 + 0.05531\,u^5 \\
&\quad +0.04061\,u^6 + 0.03075\,u^7 + 0.02386\,u^8 + 0.01888\,u^9 + 0.01520\,u^{10} \\
&\quad +0.01241\,u^{11} + 0.01026\,u^{12} + 0.008575\,u^{13} + 0.007238\,u^{14} \\
&\quad +0.006164\,u^{15} + 0.005290\,u^{16} + \mathcal{O}(u^{17})\,, \qquad (2.27)\\
C_{8,A_uA_u^\star}^{H(3),r\to \infty} &= 2.278 - 5.214\frac{1}{r} + 20.02\frac{\ln r}{r^2} - 39.76\frac{1}{r^2} + 78.58\frac{\ln r}{r^3} - 66.39\frac{1}{r^3} \\
&\quad +91.89\frac{\ln r}{r^4} + 96.35\frac{1}{r^4} - 300.7\frac{\ln r}{r^5} + 826.2\frac{1}{r^5} + \mathcal{O}\left(\frac{1}{r^6}\right), \qquad (2.28)\\
C_{8,A_dA_u^\star}^{H(3),r\to 0} &= -19.80\,r\ln^3 r - 174.7\,r\ln^2 r - 658.4\,r\ln r - 929.8\,r \\
&\quad -31.83\,r^2\ln^3 r - 612.6\,r^2\ln^2 r - 2770\,r^2\ln r - 2943\,r^2 \\
&\quad -40.68\,r^3\ln^3 r - 1439\,r^3\ln^2 r - 7906\,r^3\ln r - 6481\,r^3 \\
&\quad +54.66\,r^4\ln^3 r - 2777\,r^4\ln^2 r - 17770\,r^4\ln r - 11684\,r^4 \\
&\quad +1003\,r^5\ln^3 r - 2627\,r^5\ln^2 r - 29962\,r^5\ln r - 15962\,r^5 + \mathcal{O}(r^6)\,, \qquad (2.29)\\
C_{8,A_dA_u^\star}^{H(3),r\to 1^-} &= -0.6110 + 1.095\,\bar{u} + 0.6492\,\bar{u}^2 + 0.4596\,\bar{u}^3 + 0.3569\,\bar{u}^4 \\
&\quad +0.2910\,\bar{u}^5 + 0.2438\,\bar{u}^6 + 0.2075\,\bar{u}^7 + 0.1785\,\bar{u}^8 \\
&\quad +0.1546\,\bar{u}^9 + 0.1347\,\bar{u}^{10} + 0.1177\,\bar{u}^{11} + 0.1032\,\bar{u}^{12} \\
&\quad +0.09073\,\bar{u}^{13} + 0.07987\,\bar{u}^{14} + 0.07040\,\bar{u}^{15} + 0.06210\,\bar{u}^{16} + \mathcal{O}(\bar{u}^{17})\,, \qquad (2.30)\\
C_{8,A_dA_u^\star}^{H(3),r\to 1^+} &= -0.6110 - 1.095\,u - 0.4463\,u^2 - 0.2568\,u^3 - 0.1698\,u^4 - 0.1197\,u^5 \\
&\quad -0.08761\,u^6 - 0.06595\,u^7 - 0.05079\,u^8 - 0.03987\,u^9 - 0.03182\,u^{10} \\
&\quad -0.02577\,u^{11} - 0.02114\,u^{12} - 0.01754\,u^{13} - 0.01471\,u^{14} - 0.01244\,u^{15} \\
&\quad -0.01062\,u^{16} + \mathcal{O}(u^{17})\,, \qquad (2.31)\\
C_{8,A_dA_u^\star}^{H(3),r\to \infty} &= -3.174 + 10.89\frac{1}{r} - 35.42\frac{\ln r}{r^2} + 63.74\frac{1}{r^2} - 110.7\frac{\ln r}{r^3} + 62.26\frac{1}{r^3} \\
&\quad -71.62\frac{\ln r}{r^4} - 205.7\frac{1}{r^4} + 476.9\frac{\ln r}{r^5} - 1003\frac{1}{r^5} + \mathcal{O}\left(\frac{1}{r^6}\right). \qquad (2.32)
\end{aligned}
$$

At this point, a comment concerning the expansions in $\bar{u} = 1 - m_t^2(\mu_0)/M_{H^+}^2$ and $u = 1 - M_{H^+}^2/m_t^2(\mu_0)$ is in order. For $M_{H^+} \approx m_t$, one can expand either in $\bar{u}$ or in u, and the two expansions are easily convertible into each other.[2] As it has been observed in ref. [23], one expects better convergence of the expansion for $M_{H^+} \geq m_t$ ($M_{H^+} \leq m_t$) if the result is expressed in terms of $\bar{u}$ (u). In the following, we shall always choose the better-suited representation without explicitly mentioning it.

[2]The exact expansion coefficients from ref. [22] should be used for the conversion.

JHEP11(2012)036

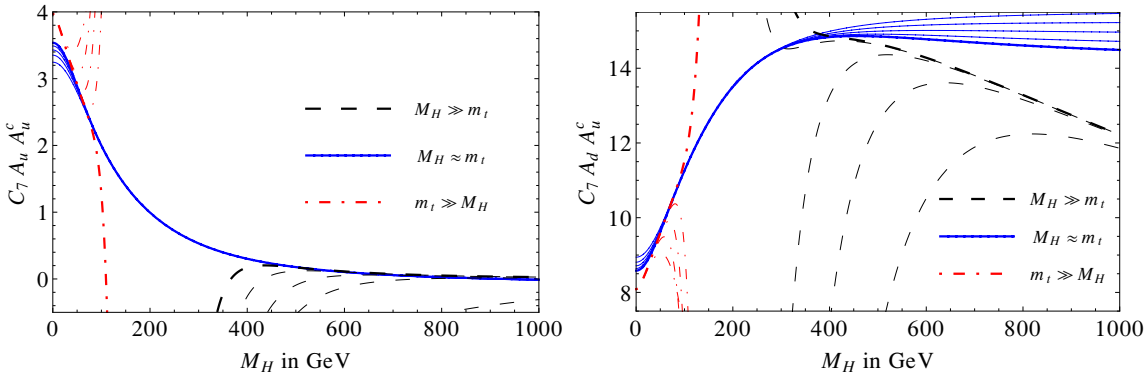

Figure 3. Three-loop coefficients $C^{H(3)}_{7,A_uA_u^\star}(\mu_0 = m_t)$ (a) and $C^{H(3)}_{7,A_dA_u^\star}(\mu_0 = m_t)$ (b) as functions of M_{H^+}. The dashed, solid and dash-dotted lines correspond to the expansions for $M_{H^+} \to \infty$, $M_{H^+} \approx m_t$ and $M_{H^+} \to 0$, respectively.

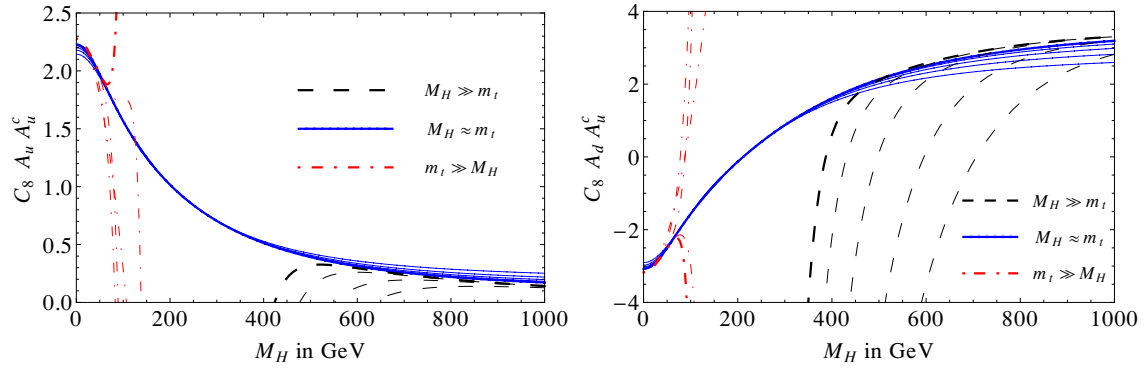

Figure 4. Three-loop coefficients $C^{H(3)}_{8,A_uA_u^\star}(\mu_0 = m_t)$ (a) and $C^{H(3)}_{8,A_dA_u^\star}(\mu_0 = m_t)$ (b) as functions of M_{H^+}. The dashed, solid and dash-dotted lines correspond to the expansions for $M_{H^+} \to \infty$, $M_{H^+} \approx m_t$ and $M_{H^+} \to 0$, respectively.

In figures 3 and 4, we demonstrate that the above expansions are sufficient to obtain the Wilson coefficients for any M_{H^+}. In figure 3(a), the coefficient $C^{H(3)}_{7,A_uA_u^\star}(\mu_0 = m_t)$ is plotted as a function of M_{H^+}. The thick-dashed, solid and dash-dotted lines show the results for $r \to 0$, $r \to 1$ and $r \to \infty$, respectively, including the highest available expansion coefficients. Convergence of the expansions is illustrated by the thin lines that describe lower orders in the respective expansions. One observes that the thick dash-dotted and solid curves overlap for $M_{H^+} \approx 30$–$70\,\text{GeV}$, which suggests that good approximations to the (unknown) exact results are provided by the $r \to \infty$ and $r \to 1$ expansions for $M_{H^+} < 50\,\text{GeV}$ and $M_{H^+} > 50\,\text{GeV}$, respectively. Similarly, for $M_{H^+} \approx 500$–$650\,\text{GeV}$, one observes agreement between the solid and dashed curves, which justifies the use of the $r \to 1$ result for $M_{H^+} < 520\,\text{GeV}$ and the $r \to 0$ result above this value. In this way, we can define $C^{H(3)}_{7,A_uA_u^\star}(\mu_0 = m_t)$ as a piecewise function using the expansions in the various

JHEP11(2012)036

limits. In figure 3(b), the corresponding results for the coefficient $C_{7,A_dA_u^\star}^{H(3)}(\mu_0 = m_t)$ are plotted showing the same features, however, with a smaller overlap of the $M_{H^+} \gg m_t$ and $M_{H^+} \approx m_t$ curves. For the phenomenological analysis in the next section, we define

$$C_{7,X}^{H(3)} = \begin{cases} C_{7,X}^{H(3)}(r \to \infty) & \text{for} \quad M_{H^+} < 50\,\text{GeV} \\ C_{7,X}^{H(3)}(r \to 1) & 50\,\text{GeV} \le M_{H^+} < M_{7,X} \\ C_{7,X}^{H(3)}(r \to 0) & M_{H^+} \ge M_{7,X} \end{cases}, \tag{2.33}$$

with $M_{7,A_uA_u^\star} = 520\,\text{GeV}$ and $M_{7,A_dA_u^\star} = 400\,\text{GeV}$.

Analogous results for $C_8^{H(3)}(\mu_0 = m_t)$ are shown in figure 4. We observe the same pattern as for $C_7^{H(3)}(\mu_0 = m_t)$, which leads us to define

$$C_{8,X}^{H(3)} = \begin{cases} C_{8,X}^{H(3)}(r \to \infty) & \text{for} \quad M_{H^+} < 50\,\text{GeV} \\ C_{8,X}^{H(3)}(r \to 1) & 50\,\text{GeV} \le M_{H^+} < M_{8,X} \\ C_{8,X}^{H(3)}(r \to 0) & M_{H^+} \ge M_{8,X} \end{cases}, \tag{2.34}$$

with $M_{8,A_uA_u^\star} = 600\,\text{GeV}$ and $M_{8,A_dA_u^\star} = 520\,\text{GeV}$.

The `Mathematica` file in ref. [22] contains the definitions (2.33) and (2.34), which allows for convenient numerical evaluation of the 2HDM contributions to C_7 and C_8. The updated SM results are included there, too.

3 $\mathcal{B}(\bar{B} \to X_s\gamma)$ in the 2HDM to NNLO

The framework for our numerical analysis is based on ref. [9] where explicit results for the effective-theory description of $\mathcal{B}(\bar{B} \to X_s\gamma)$ have been provided up to the NNLO. While the Wilson coefficients are known in a complete manner at this order, non-BLM NNLO corrections to the charm-quark-mass-dependent matrix elements (on-shell amplitudes) have been evaluated only in the large m_c limit and extrapolated to the physical region.

Predictions within the 2HDM to be discussed below are obtained along the same algorithm and using the complete NNLO matching conditions from the previous section. However, two-loop purely electroweak corrections to the matching are included in the SM part only, as they remain unknown in the 2HDM. One should keep in mind that such electroweak corrections and our new NNLO QCD matching ones may be of comparable size.

In the following, we shall discuss results for the 2HDMs of type-I and II that have been introduced in eqs. (2.8) and (2.9). Most of the input parameters are adopted from ref. [9], except for the strong coupling constant and the top quark mass for which we use the most up-to-date values that are given by [24–26].[3]

$$\begin{aligned} \alpha_s(M_Z) &= 0.1184 \pm 0.0014\,, \\ M_t &= (173.18 \pm 0.56_{\text{stat}} \pm 0.75_{\text{syst}})\,\text{GeV}. \end{aligned} \tag{3.1}$$

[3] Conservatively, we use "0.0014" as the uncertainty for α_s instead of "0.0007" [25, 26]. This is motivated by the current tension in several precision determinations of α_s (see discussion in ref. [27]).

JHEP11(2012)036

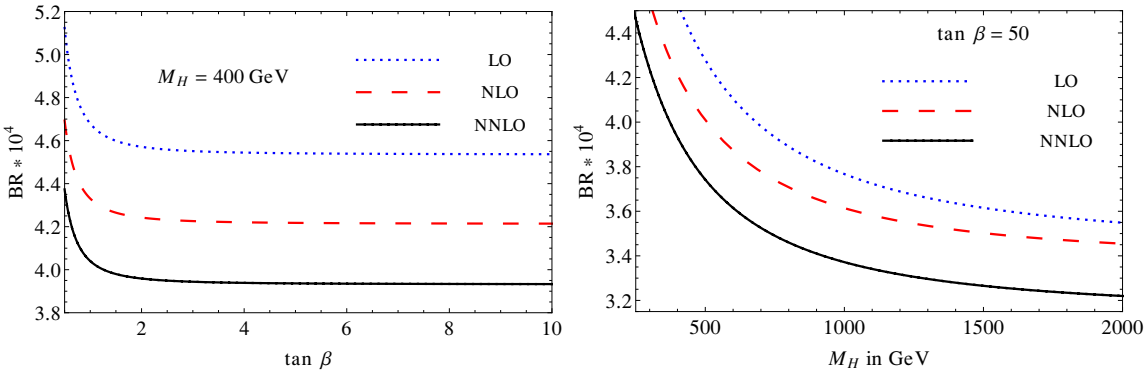

Figure 5. $\mathcal{B}(\bar{B} \to X_s\gamma)$ in the 2HDM type-II as a function of $\tan\beta$ for $M_{H^+} = 400\,\text{GeV}$ (left plot), and as a function of M_{H^+} for $\tan\beta = 50$ (right plot). Dotted, dashed and solid lines show central values (without uncertainties) of the LO, NLO and NNLO results, respectively.

The corresponding $\overline{\text{MS}}$ top quark mass equals $m_t(m_t) = 163.5\,\text{GeV}$ using three-loop accuracy in QCD [28, 29] and neglecting electroweak effects. As in ref. [9], our default value of the photon energy cut is $E_0 = 1.6\,\text{GeV}$. Furthermore, if not stated otherwise, we choose $\mu_0 = 160\,\text{GeV}$, $\mu_b = 2.5\,\text{GeV}$ and $\mu_c = 1.5\,\text{GeV}$ for the renormalization scales, where μ_0 is the matching scale, μ_b is the scale at which on-shell matrix elements in the effective theory are evaluated, and μ_c is the charm quark mass renormalization scale.

In a first step, let us discuss the branching ratio dependence on $\tan\beta$. In figure 5(a), we choose $M_{H^+} = 400\,\text{GeV}$ and show $\mathcal{B}(\bar{B} \to X_s\gamma)$ in the 2HDM type-II for $0.5 \leq \tan\beta \leq 10$. The solid curve describes the NNLO result, while the dotted and dashed ones show the LO and NLO central values for comparison. One observes strong dependence for $\tan\beta < 2$ and a nearly $\tan\beta$-independent result for $\tan\beta > 2$. Actually, from $\tan\beta = 10$ to $\tan\beta = 50$, the branching ratio changes only by 0.03%. In the following, $\tan\beta = 50$ is going to be our default value for the type-II model; choosing $\tan\beta < 2$ would strengthen the lower limit on M_{H^+}.

In figure 5(b), we show $\mathcal{B}(\bar{B} \to X_s\gamma)$ in the same model with $\tan\beta = 50$ as a function of M_{H^+}. As expected, for large values of M_{H^+}, the 2HDM result approaches the SM one that overlaps with the bottom frame of the plot in the NNLO case. For $M_{H^+} = 300\,\text{GeV}$ the NNLO curve overshoots the SM prediction by about 35%, while the effect decreases to around 2% at $M_{H^+} = 2\,\text{TeV}$.

The main effect of our new three-loop terms is in reducing μ_0-dependence of the decay rate and, in consequence, stabilizing the lower bound on M_{H^+}. This is illustrated in figure 6(a) where the charged Higgs contribution to the branching ratio $\Delta\mathcal{B} \equiv \mathcal{B}_{\text{2HDM}} - \mathcal{B}_{\text{SM}}$ is plotted as a function of μ_0, while normalized to its own value at $\mu_0 = M_{H^+} = 400\,\text{GeV}$. Apart from the LO (dotted), NLO (dashed), NNLO (solid) curves, we also present the partial NNLO (dash-dotted) line that corresponds to the approach of ref. [10]. Our calculation differs from the latter one precisely by including the 2HDM contributions to the NNLO matching. One observes a clear reduction of μ_0-dependence when including

JHEP11(2012)036

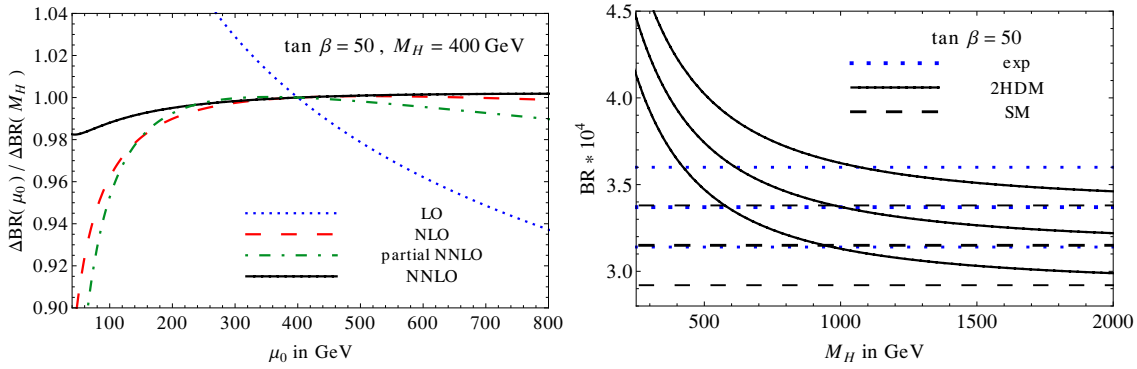

(a) (b)

Figure 6. A closer look at the 2HDM type-II results. Left: $\Delta\mathcal{B}(\mu_0)/\Delta\mathcal{B}(\mu_0 = M_{H^+})$ as a function of μ_0 for $\tan\beta = 50$ and $M_{H^+} = 400\,\text{GeV}$ at the LO (dotted), NLO (dashed) and NNLO (solid). Dash-dotted lines correspond to the partial NNLO result which has been used in ref. [10]. Right: $\mathcal{B}(\bar{B} \to X_s\gamma)$ as a function of M_{H^+} for $\tan\beta = 50$. Middle lines show the central values, while the upper and lower ones are shifted by $\pm 1\sigma$. Solid and dashed lines correspond to the NNLO 2HDM and SM predictions, respectively. Dotted curves represent the experimental average in eq. (1.1).

higher order corrections. Whereas the partial NNLO result for the considered ratio varies by more than 6.6% when μ_0 is varied in the $[80\,\text{GeV}, 2M_{H^+}]$ range, the corresponding variation of our present result with full NNLO matching remains below 1.6%. The overall size of $\Delta\mathcal{B}(\mu_0)$ amounts to around 25% of $\mathcal{B}(\bar{B} \to X_s\gamma)_{\text{SM}}$ in the considered case.

In order to determine a lower bound on M_{H^+} we follow the approach of ref. [10], combining the experimental and theoretical uncertainties in quadrature. A one-sided 95% C.L. (99% C.L.) bound is obtained for the lowest value of M_{H^+} for which the difference between experimental and theoretical central values is 1.645 (2.326) times larger than the total uncertainty.

The theory uncertainty consists of four contributions that we take over from ref. [9]. Let us briefly comment on each of them:

- In ref. [9], the non-perturbative uncertainty has been estimated to $\pm 5\%$, which has been confirmed by the detailed investigation of ref. [30]. We adopt this uncertainty for all the considered values of M_{H^+}.

- The charm quark mass dependence of the operator matrix elements is only partly known. Thus, an interpolation between the large-m_c results [31] and reasonable assumptions for $\mathcal{B}(\bar{B} \to X_s\gamma)$ at $m_c = 0$ has to be performed. This uncertainty has been estimated in [9] to $\pm 3\%$, which we again assume to be M_{H^+}-independent.

- The total parametric error is obtained by combining all the partial ones in quadrature.[4] It amounts to around $2 \div 3\%$, however, computed from scratch for each value of M_{H^+}.

[4] A correlation between the phase space factor C and m_c is taken into account as described in appendix A of ref. [9].

JHEP11(2012)036

- An estimate of higher order corrections is obtained by varying the renormalization scales in the ranges $80\,\text{GeV} \leq \mu_0 \leq \max\{2M_{H^+}, 320\,\text{GeV}\}$, $1.25\,\text{GeV} \leq \mu_b \leq 5\,\text{GeV}$ and $1.224\,\text{GeV} \leq \mu_c \leq M_b^{1S} = 4.68\,\text{GeV}$. This uncertainty is about $3 \div 4\%$ but again we compute it for each value of M_{H^+}.

Contrary to refs. [9, 10], we work with asymmetric uncertainties resulting from the parameter and renormalization scale variation.

In figure 6(b), the NNLO result for $\mathcal{B}(\bar{B} \to X_s\gamma)$ is shown as a function of M_{H^+}, together with an uncertainty band that is obtained by adding all the errors in quadrature. The dotted (M_{H^+}-independent) curves in figure 6(b) correspond to the experimental result in eq. (1.1). For comparison, we also show the SM prediction with the corresponding uncertainty as dashed lines.

From figure 6(b) one can extract (using the procedure described above) the following limits on M_{H^+} in the 2HDM type-II:

$$\begin{aligned} M_{H^+} &\geq 380\,\text{GeV} \quad \text{at } 95\%\,\text{C.L.}\,, \\ M_{H^+} &\geq 289\,\text{GeV} \quad \text{at } 99\%\,\text{C.L.}\,. \end{aligned} \tag{3.2}$$

The above bounds replace the ones of ref. [10] (295 and 230 GeV, respectively). A considerable improvement of the bounds arises mostly due to the shift in the experimental value of $\mathcal{B}(\bar{B} \to X_s\gamma)$ that is now smaller than the one used in ref. [10]. Our 95% C.L. limit is very close to the one presented in ref. [8] (385 GeV) together with the new experimental average (eq. (1.1)). On the other hand, it is significantly stronger than the one in refs. [4, 5] (327 GeV) that is based on the BABAR data alone. It is interesting to mention that when the matching scale μ_0 is varied between 80 and 400 GeV, the lower limits vary by around 25 GeV when our new three-loop 2HDM matching contributions are *not* included. This gets reduced to around 7 GeV only after including the three-loop corrections, which demonstrates the stabilizing effect of the full NNLO matching. On the other hand, for $\mu_0 = 160\,\text{GeV}$ fixed, the correction strengthens the limit only slightly, by $5 \div 6\,\text{GeV}$.

The contour plots in figure 7 show the 95% C.L. lower bounds on M_{H^+} as functions of the experimentally determined branching ratio and the corresponding uncertainty. Black dots correspond to the result in eq. (1.1), while the two black lines at the bottom indicate the projected uncertainty to be reached by Belle II and SuperB [32]. The current theory uncertainty has been used in figure 7(a), while figure 7(b) presents a future projection with assumed reduction of the theory uncertainty by a factor of two.

Let us now shortly discuss the 2HDM of type-I. In figure 8(a), we show the branching ratio for $\tan\beta = 1$ as a function of M_{H^+}, including the uncertainties. The meaning of the curves is the same as in figure 6(b). Contrary to the type-II model, the branching ratio gets suppressed with respect to the SM, and the effect becomes larger for lower values of M_{H^+}, which implies increased discrepancy with respect to the experimental results. Thus, it is possible to set a lower bound on M_{H^+}. It is shown in figure 8(b) where the shaded area represents the part of the $\tan\beta$-M_{H^+} plane that is excluded at 95% C.L. Similar results based on the partial NNLO predictions and the previous experimental average have been presented in ref. [33].

JHEP11(2012)036

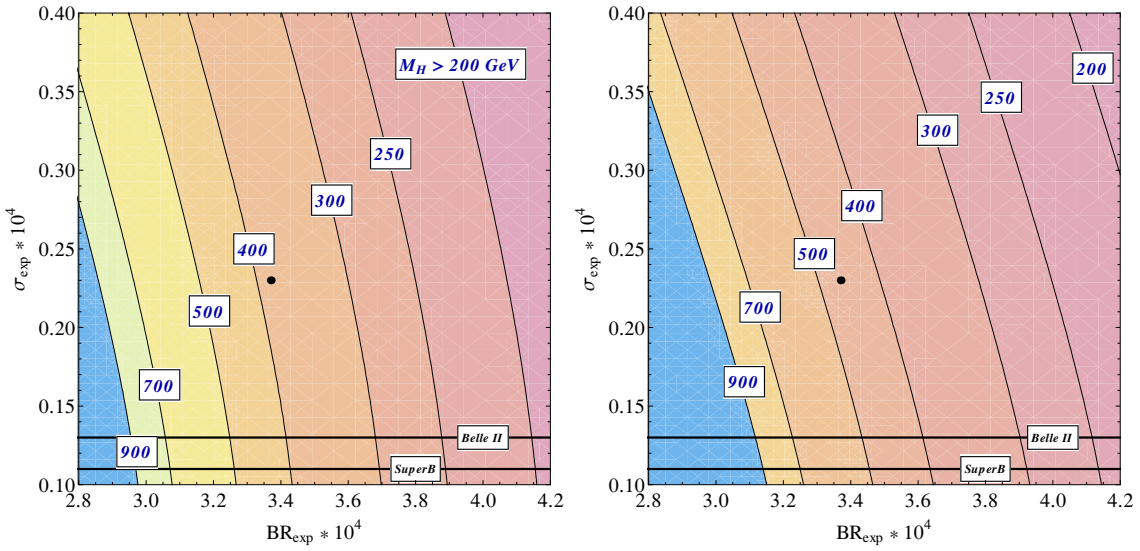

(a) (b)

Figure 7. Lower bounds on M_{H^+} at the 95% C.L. as a function of the experimentally determined branching ratio (abscissa) and the corresponding uncertainty (ordinate). The current theory uncertainty has been used in panel (a), while panel (b) presents a future projection with assumed reduction of the theory uncertainty by a factor of two.

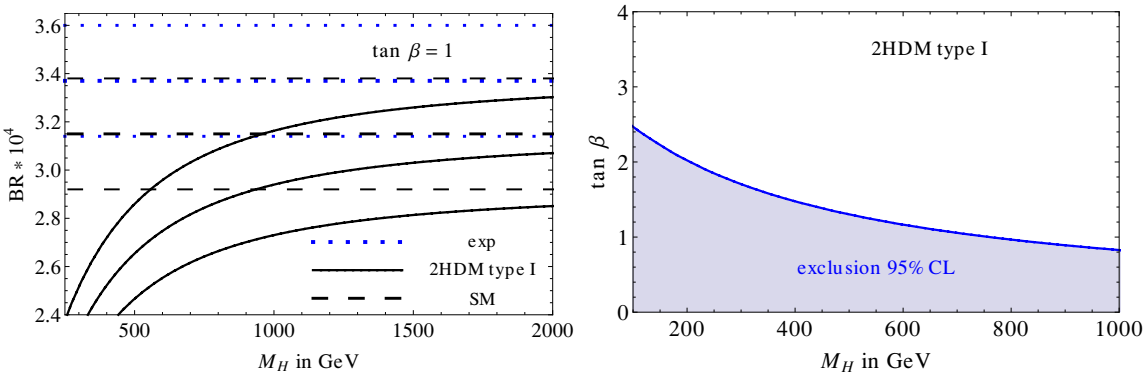

(a) (b)

Figure 8. Left: $\mathcal{B}(\bar{B} \to X_s\gamma)$ for 2HDM type-I with $\tan\beta = 1$. Identification of the lines is the same as in figure 6(b). Right: 95% C.L. exclusion (shaded area) for 2HDM type-I in the plane of $\tan\beta$ and M_{H^+}.

4 Conclusions

Applying the method of expansion in mass ratios, we have evaluated three-loop matching conditions for the dipole operators P_7 and P_8 in the 2HDM. In effect, Wilson coefficients of all the operators that matter for $\bar{B} \to X_s\gamma$ in this model at the leading order in electroweak interactions are now known to the NNLO accuracy in QCD. This is true not only at the matching scale μ_0 but also at the low-energy scale μ_b because the renormalization group evolution is the same as in the SM [34].

JHEP11(2012)036

The main effect of including the NNLO matching is a significant reduction of μ_0-dependence of the charged Higgs contribution to the $\bar{B} \to X_s\gamma$ branching ratio. It is particularly transparent when considering a lower bound on M_{H^+} in the type-II model. Before taking our correction into account, the bound varies by around 25 GeV when μ_0 is varied in a reasonable range $[80, 400]\,\text{GeV} \sim [\frac{1}{2}m_t, M_{H^+}]$. Including the correction reduces the variation by more than a factor of 3.

With the updated experimental average, we find that the 95% C.L. (99% C.L.) lower limit on M_{H^+} amounts to 380 (289) GeV in the 2HDM type-II. This is a universal ($\tan\beta$-independent) bound that can only get stronger when $\tan\beta$-dependence is taken into account. In practice, noticeable modifications occur for $\tan\beta$ smaller than around 2.

In the 2HDM type-I, a 95% C.L. lower limit on M_{H^+} from $\mathcal{B}(\bar{B} \to X_s\gamma)$ can be derived for low $\tan\beta$ only, currently for $\tan\beta < 2.5$ when M_{H^+} is above the LEP bound of around 80 GeV [25]. In this case, considerable reduction of μ_0-dependence is observed, too.

With the semi-analytical results presented in this paper, constraints on the 2HDM at the NNLO level can easily be updated in the future, along with developments in the measurements and in calculations of the low-energy matrix elements (that are identical in the SM and in the 2HDM). More precise measurements are expected in a few years from Belle-II [35] and Super-B [36]. On the theoretical side, the main challenges are improvements in analyses of non-perturbative effects [30] together with perturbative calculations of the NNLO on-shell amplitudes beyond the large-m_c limit. In the latter case, new results should become available soon [37].

Acknowledgments

This work has been supported by the DFG through the SFB/TR 9 "Computational Particle Physics" and the Graduiertenkolleg "Elementarteilchenphysik bei höchster Energie und höchster Präzision". M.M. acknowledges partial support from the National Science Centre (Poland) research project, decision no DEC-2011/01/B/ST2/00438, as well as from the DFG through the "Mercator" guest professorship programme.

Note added. Shortly after our paper had been submitted, a new experimental value for the branching ratio $\mathcal{B}(\bar{B} \to X_s\gamma)|_{E_\gamma > 1.6\,\text{GeV}} = (3.43 \pm 0.22) \times 10^{-4}$ appeared at the HFAG web page [38]. If this result was used instead of eq. (1.1), our bounds in eq. (3.2) would read

$$M_{H^+} \geq 360\,\text{GeV} \quad \text{at } 95\%\,\text{C.L.}\,,$$
$$M_{H^+} \geq 277\,\text{GeV} \quad \text{at } 99\%\,\text{C.L.}\,.$$

JHEP11(2012)036

References

[1] CLEO collaboration, S. Chen et al., *Branching fraction and photon energy spectrum for $b \to s\gamma$*, *Phys. Rev. Lett.* **87** (2001) 251807 [hep-ex/0108032] [INSPIRE].

[2] BELLE collaboration, K. Abe et al., *A measurement of the branching fraction for the inclusive $B \to X_s\gamma$ decays with BELLE*, *Phys. Lett.* **B 511** (2001) 151 [hep-ex/0103042] [INSPIRE].

[3] BELLE collaboration, A. Limosani et al., *Measurement of inclusive radiative B-meson decays with a photon energy threshold of 1.7 GeV*, *Phys. Rev. Lett.* **103** (2009) 241801 [arXiv:0907.1384] [INSPIRE].

[4] BABAR collaboration, J.P. Lees et al., *Precision measurement of the $B \to X_s\gamma$ photon energy spectrum, branching fraction and direct CP asymmetry $A_{CP}(B \to X_{s+d}\gamma)$*, arXiv:1207.2690 [INSPIRE].

[5] BABAR collaboration, J. Lees, V. Poireau and V. Tisserand, *Measurement of $B(B \to X_s\gamma)$, the $B \to X_s\gamma$ photon energy spectrum and the direct CP asymmetry in $B \to X_{s+d}\gamma$ decays*, arXiv:1207.5772 [INSPIRE].

[6] BABAR collaboration, J.P. Lees et al., *Exclusive measurements of $b \to s\gamma$ transition rate and photon energy spectrum*, *Phys. Rev.* **D 86** (2012) 052012 [arXiv:1207.2520] [INSPIRE].

[7] BABAR collaboration, B. Aubert et al., *Measurement of the $B \to X_s\gamma$ branching fraction and photon energy spectrum using the recoil method*, *Phys. Rev.* **D 77** (2008) 051103 [arXiv:0711.4889] [INSPIRE].

[8] S. Stone, *New physics from flavour*, talk given at the *International Conference on High Energy Physics (ICHEP 2012)*, Melbourne Australia, 4–11 Jul 2012.

[9] M. Misiak and M. Steinhauser, *NNLO QCD corrections to the $\bar{B} \to X_s\gamma$ matrix elements using interpolation in m_c*, *Nucl. Phys.* **B 764** (2007) 62 [hep-ph/0609241] [INSPIRE].

[10] M. Misiak et al., *Estimate of $B(\bar{B} \to X_s\gamma)$ at $O(\alpha_s^2)$*, *Phys. Rev. Lett.* **98** (2007) 022002 [hep-ph/0609232] [INSPIRE].

[11] S.L. Glashow and S. Weinberg, *Natural conservation laws for neutral currents*, *Phys. Rev.* **D 15** (1977) 1958 [INSPIRE].

[12] H. Flächer et al., *Revisiting the global electroweak fit of the standard model and beyond with Gfitter*, *Eur. Phys. J.* **C 60** (2009) 543 [*Erratum ibid.* **C 71** (2011) 1718] [arXiv:0811.0009] [INSPIRE].

[13] C. Bobeth, M. Misiak and J. Urban, *Photonic penguins at two loops and m_t-dependence of* BR$[B \to X_s l^+ l^-]$, *Nucl. Phys.* **B 574** (2000) 291 [hep-ph/9910220] [INSPIRE].

[14] M. Misiak and M. Steinhauser, *Three loop matching of the dipole operators for $b \to s\gamma$ and $b \to sg$*, *Nucl. Phys.* **B 683** (2004) 277 [hep-ph/0401041] [INSPIRE].

[15] A.J. Buras and M. Misiak, *$\bar{B} \to X_s\gamma$ after completion of the NLO QCD calculations*, *Acta Phys. Polon.* **B 33** (2002) 2597 [hep-ph/0207131] [INSPIRE].

[16] M. Ciuchini, G. Degrassi, P. Gambino and G.F. Giudice, *Next-to-leading QCD corrections to $B \to X_s\gamma$: standard model and two Higgs doublet model*, *Nucl. Phys.* **B 527** (1998) 21 [hep-ph/9710335] [INSPIRE].

[17] F. Borzumati and C. Greub, *2HDMs predictions for $\bar{B} \to X_s\gamma$ in NLO QCD*, *Phys. Rev.* **D 58** (1998) 074004 [hep-ph/9802391] [INSPIRE].

JHEP11(2012)036

[18] F. Borzumati and C. Greub, *Two Higgs doublet model predictions for $\bar{B} \to X_s\gamma$ in NLO QCD: addendum*, *Phys. Rev.* **D 59** (1999) 057501 [hep-ph/9809438] [INSPIRE].

[19] P. Ciafaloni, A. Romanino and A. Strumia, *Two loop QCD corrections to charged Higgs mediated $b \to s\gamma$ decay*, *Nucl. Phys.* **B 524** (1998) 361 [hep-ph/9710312] [INSPIRE].

[20] C. Bobeth, M. Misiak and J. Urban, *Matching conditions for $b \to s\gamma$ and $b \to s$ gluon in extensions of the standard model*, *Nucl. Phys.* **B 567** (2000) 153 [hep-ph/9904413] [INSPIRE].

[21] C. Bobeth, A.J. Buras and T. Ewerth, *$\bar{B} \to X_s\ell^+\ell^-$ in the MSSM at NNLO*, *Nucl. Phys.* **B 713** (2005) 522 [hep-ph/0409293] [INSPIRE].

[22] www-ttp.particle.uni-karlsruhe.de/Progdata/ttp12/ttp12-29/.

[23] D. Eiras and M. Steinhauser, *Complete Higgs mass dependence of top quark pair threshold production to order $\alpha\alpha_s$*, *Nucl. Phys.* **B 757** (2006) 197 [hep-ph/0605227] [INSPIRE].

[24] CDF and D0 collaborations, T. Aaltonen et al., *Combination of the top-quark mass measurements from the Tevatron collider*, arXiv:1207.1069 [INSPIRE].

[25] Particle Data Group collaboration, J. Beringer et al., *Review of particle physics (RPP)*, *Phys. Rev.* **D 86** (2012) 010001 [INSPIRE].

[26] S. Bethke, *World summary of α_s (2011)*, *Nucl. Phys. Proc. Suppl.* **222-224** (2012) 94 [INSPIRE].

[27] S. Bethke et al., *Workshop on precision measurements of α_s*, arXiv:1110.0016 [INSPIRE].

[28] K.G. Chetyrkin and M. Steinhauser, *The relation between the $\overline{\rm MS}$ and the on-shell quark mass at order α_s^3*, *Nucl. Phys.* **B 573** (2000) 617 [hep-ph/9911434] [INSPIRE].

[29] K. Melnikov and T. van Ritbergen, *The three loop relation between the $\overline{\rm MS}$ and the pole quark masses*, *Phys. Lett.* **B 482** (2000) 99 [hep-ph/9912391] [INSPIRE].

[30] M. Benzke, S.J. Lee, M. Neubert and G. Paz, *Factorization at subleading power and irreducible uncertainties in $\bar{B} \to X_s\gamma$ decay*, *JHEP* **08** (2010) 099 [arXiv:1003.5012] [INSPIRE].

[31] M. Misiak and M. Steinhauser, *Large-m_c asymptotic behaviour of $O(\alpha_s^2)$ corrections to $B \to X_s\gamma$*, *Nucl. Phys.* **B 840** (2010) 271 [arXiv:1005.1173] [INSPIRE].

[32] B. Meadows et al., *The impact of SuperB on flavour physics*, arXiv:1109.5028 [INSPIRE].

[33] F. Mahmoudi and O. Stal, *Flavor constraints on the two-Higgs-doublet model with general Yukawa couplings*, *Phys. Rev.* **D 81** (2010) 035016 [arXiv:0907.1791] [INSPIRE].

[34] M. Czakon, U. Haisch and M. Misiak, *Four-loop anomalous dimensions for radiative flavour-changing decays*, *JHEP* **03** (2007) 008 [hep-ph/0612329] [INSPIRE].

[35] Belle II collaboration, T. Abe, *Belle II technical design report*, arXiv:1011.0352 [INSPIRE].

[36] SuperB collaboration, B. O'Leary et al., *SuperB progress reports — physics*, arXiv:1008.1541 [INSPIRE].

[37] M. Misiak, *QCD challenges in radiative B decays*, *AIP Conf. Proc.* **1317** (2011) 276 [arXiv:1010.4896] [INSPIRE].

[38] http://www.slac.stanford.edu/xorg/hfag/.

JHEP11(2012)036